# Properties and Aging of Bottom-Contact CuO/Au Transmission Line Model (TLM) Structures

Xi Zeng, Maria Zhukova, Sébastien Faniel, Guoli Li, and Denis Flandre, *Senior Member, IEEE*

***Abstract*— The bottom-contact CuO/Au transmission line model (TLM) structures have been fabricated and measured both in $N_2$ and vacuum for the first time to obtain a cleaner CuO/Au interface by avoiding the exposure of the interface to the ambiance, compared to top-contact structures. Considering different strip widths, CuO/Au TLM structures measured in $N_2$ show typical width-normalized contact resistances ($R_C \cdot W$) of ∼2.6 kΩ·cm, which is relatively low compared to the total resistance of CuO. The linearity of *I–V* curves further indicates an ohmic contact between Au and CuO. All the CuO/Au TLM structures measured in $N_2$ right after fabrication show repeatable and reliable effective contact resistivities ($\rho_{C\text{-}eff}$) of ∼0.55 Ω·cm$^2$ regardless of the increased $R_C$ with decreasing CuO widths. Measured in vacuum, other thinner, more resistive CuO/Au TLM structures fabricated by the same processes exhibit lower $R_C \cdot W$ of ∼1.8 kΩ·cm and record low $\rho_{C\text{-}eff}$ of ∼0.05 Ω·cm$^2$ that might be related to the reduction of the transfer length with the increase of the CuO sheet resistance. Further investigating the CuO/Au TLM structures, the degradations of sheet and contact resistances have been observed along time for the first time when measuring the devices in vacuum at room temperature. Such aging is significantly accelerated at 100 °C. The lack of stability of CuO/Au contacts we investigated might shine some light on the discrepancy of results widely reported in literature.**

***Index Terms*— Aging, bottom contact, contact resistance, CuO, degradation, transmission line model (TLM) structure.**

## I. Introduction

METAL–SEMICONDUCTOR contact is a vital element for any semiconductor device. The contact resistance ($R_c$) significantly affects the injection and extraction efficiencies of charge carriers at the metal–semiconductor interface and plays a notable role in the electrical performances of thin-film transistors (TFTs) [1], [2]. Especially for short-channel TFTs, the contact resistance could become dominant in the transistor performances [3], [4]. To optimize the design of TFTs, an ohmic contact with a low $R_c$ is always expected. The transmission line model (TLM) structure, which consists of various metal grids with unequal spacing between contacts, is one of the commonly used methods to determine the contact characteristics [5].

As one of the most promising p-type metal–oxide–semiconductors, CuO thin films have been successfully fabricated and characterized on glass [6]. Since CuO typically has a high work function over 5.19 eV [7], Au is normally selected as the metal contact due to its high work function up to 5.47 eV [8] and thus potential to form an ohmic contact with CuO. Nevertheless, as-fabricated CuO TFTs usually exhibit relatively low field-effect mobilities of ∼$10^{-4}$–$10^{-1}$ cm$^2$·V$^{-1}$·s$^{-1}$ [9], [10], [11]. The contact between CuO and metal could be a possible origin of carrier injection limitation [12].

As a quantitative reference, when achieving an ohmic contact to n- or p-type Si with W (tungsten), the contact resistivity ($\rho_c$) typically ranges from $10^{-8}$ to $10^{-3}$ Ω·cm$^2$ [13]. In comparison, in [14], CuO prepared by chemical reaction exhibited a very high $\rho_c$ of about $10^5$ Ω·cm$^2$ with Au. Another RF-sputtered $Cu_2O$ exhibited a high $R_c$ of 2.34 MΩ with Au [15]. $\rho_c$ was lowered by increasing the thickness of RF-sputtered copper oxides in the case of $Cu_2O$/Ni/Au TLM structures [12]. The $\rho_c$ values of CuO and $Cu_2O$ prepared by MOCVD were, respectively, $1.45 \times 10^3$ and $2.1 \times 10^3$ Ω·cm$^2$ with Au in [16]. As a reference, the lowest $\rho_c$ of $2.15 \times 10^{-5}$ Ω·cm$^2$ was reported for electrodeposited $Cu_2O$ with Ti/Au contact for a very thick film of 10 μm in [17], but it remains challenging to reduce the contact resistivity of CuO with other metals. These previously reported TLM structures were all top-contacted with metal electrodes on top of copper oxides. In contrast, bottom-contact structures are expected to exhibit a lower contact resistance due to the direct contact of the semiconductor with the metal, as well as a clean interface to limit the exposure of the contact interface to the ambiance [18].

In this work, to optimize the CuO/Au contact resistivity toward less than 1 Ω·cm$^2$ as conventionally achieved with other TFT materials, the contact properties between CuO and Au are further investigated. First, the bottom-contact CuO/Au TLM structures are fabricated and measured for the first time. The sheet ($R_{sh}$) and contact ($R_c$) resistance properties are characterized both in $N_2$ ambient and vacuum considering different structure dimensions, such as metal strip widths, CuO

Manuscript received 16 June 2024; revised 5 August 2024; accepted 6 August 2024. This work was supported by China Scholarship Council and Université Catholique de Louvain Co-Funding Fellowship under Grant CSC201806130158. The review of this article was arranged by Editor E. A. Gutiérrez-D. *(Corresponding author: Xi Zeng.)*

Xi Zeng, Maria Zhukova, Sébastien Faniel, and Denis Flandre are with the Institute of Information and Communication Technologies, Electronics and Applied Mathematics, Université Catholique de Louvain, 1348 Ottignies-Louvain-la-Neuve, Belgium (e-mail: xi.zeng@uclouvain.be).

Guoli Li is with the School of Physics and Electronics, Hunan University, Changsha 410082, China.

Color versions of one or more figures in this article are available at https://doi.org/10.1109/TED.2024.3441565.

Digital Object Identifier 10.1109/TED.2024.3441565

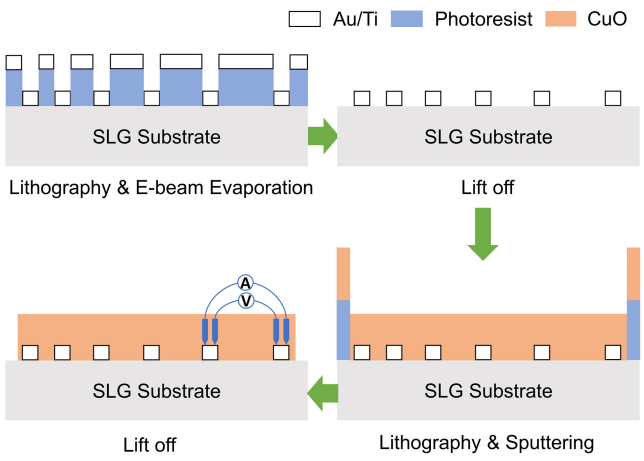


Fig. 1. Cross-sectional schematic views for the fabrication processes and measurement setups of CuO/Au TLM structures with bottom contacts (the white, blue, and orange areas are Au/Ti, photoresist, and CuO, respectively).

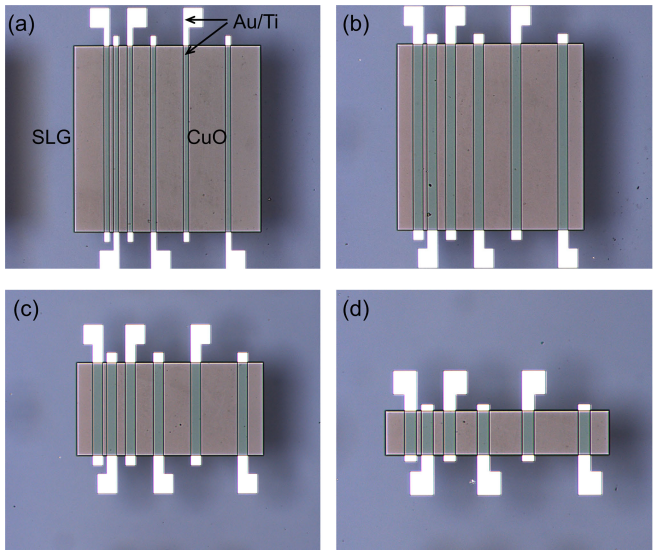


Fig. 2. Top-viewed optical microscope photographs of CuO/Au TLM structures on SLG substrates (the brown and white/greenish areas are CuO and Au, respectively). (a) Structure A. (b) Structure B. (c) Structure C. (d) Structure D.

width, and the CuO thickness. Second, the degradations of CuO sheet resistance and its contact resistance with Au are observed with aging (in over periods of several hours) for the first time and analyzed in vacuum at room and elevated (100 °C) temperatures. Finally, potential physical phenomena are discussed.

## II. Device Structures and Fabrication Details

The cross-sectional schematic views for the fabrication processes and measurement setups of the CuO/Au TLM structures are shown in Fig. 1. Soda lime glass (SLG) substrates with a size of 4 × 4 $cm^2$ were cleaned by acetone, methanol, isopropanol, and deionized water, and dried by nitrogen. UV reverse lithography was first done to define the metal contact patterns. Au/Ti (10/100 nm) strip lines were e-beam evaporated, where Ti (10 nm) was deposited between the SLG substrates and Au to enhance the adhesion of Au on glass. The samples were later placed in the acetone for lift-off. UV reverse lithography and lift-off were also used next on top of the Au/Ti contacts to pattern the CuO films deposited by dc reactive magnetron sputtering (AJA sputtering system) [6]. A constant sputtering power of 50 W was set in the chamber at a sputtering pressure of 10 m·Torr with an $O_2$/Ar ratio of 8/22 sccm. To increase the CuO thickness and achieve a lower total resistance for TLM structures, samples were sputtered at a long time of 5 h. Postannealing was carried out in $N_2$ ambient for 30 min at 250 °C. To avoid the influence of subsequent processing on the CuO surface especially for the high-temperature processes in the lithography, metal strips were fabricated first, with the CuO process steps as the final ones. To minimize the influence of internal resistance from the probes and measurement system, four-probe measurements were carried out on a LakeShore CPX probe station connected to a Keithley 4200-SCS semiconductor characterization system under dark. The leakage currents of all source-measure units (SMUs) were measured at a pA current level from −10 to 10 V. CuO/Au TLM samples were measured either in $N_2$ flow ambient or in vacuum after a pumping of 2 h.

Four as-fabricated bottom-contact TLM structures with different dimensions are presented in Fig. 2, showing the top-viewed photographs of CuO TLM structures obtained by an optical microscope (Zeiss Axio Imager Vario). These structures feature the same increasing strip distance ($d$) of 25, 50, 100, 150, and 200 $\mu$m. Structures A and B have the same CuO width ($W$) of 1000 $\mu$m but different electrode widths ($L$) of 25 and 50 $\mu$m, respectively. Structures B–D have the same $L$ of 50 $\mu$m but varying $W$ of 200, 500, and 1000 $\mu$m, respectively. In this work, these structures were fabricated by the same above processes on two samples with CuO thicknesses of 830 and 750 nm, respectively. These four structures are each repeated three times on the same chip, and necessary tests were conducted to confirm the repeatability and reliability of the measurements.

## III. TLM Characterization Results

Fig. 3 gives the top-viewed schematic of typical TLM structures with increasing strip distance ($d$) from $d_1$ to $d_5$ for contact strips $S_1$–$S_6$. The total resistance ($R_T$) between each pair of adjacent strips is obtained from three-point derivatives of current–voltage ($I$–$V$) measurements (in our case, in the range from −1 to 1 V). Upon flowing from one electrode to the other, the current successively passes through Au metal electrode, CuO/Au contact, CuO layer, and again CuO/Au contact and Au electrode. Accordingly, $R_T$ can be modeled as

$$R_T = 2R_c + R_{\text{metal}} + R_{\text{semi}} \approx 2R_c + R_{\text{sh}}\frac{d}{W} \quad (1)$$

where the metal line resistance ($R_{\text{metal}}$) is much smaller than the semiconductor resistance ($R_{\text{semi}}$) and can thus be neglected. $R_{\text{sh}} = (\rho/t)$, where $\rho$ is the CuO resistivity in Ω·cm and $t$ is the CuO thickness.

By plotting $R_T$ as a function of $d$, several parameters can be extracted from the slope, $x$-intercept ($x_{\text{intercept}}$) or y-intercept

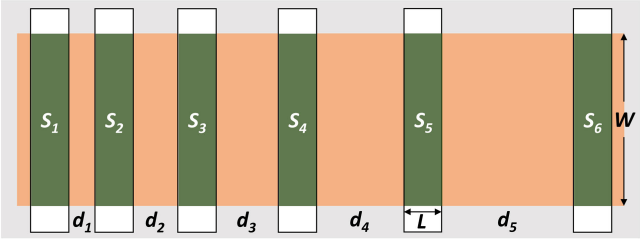


Fig. 3. Top-viewed schematic of typical TLM structures (the orange and white/green areas denote CuO and Au, respectively).

($y_{\text{intercept}}$) of the linear fitting, as follows:

$$R_{\text{sh}} = \text{slope} \times W \tag{2}$$

$$L_T = 0.5 \times x_{\text{intercept}} \tag{3}$$

$$R_c = 0.5 \times y_{\text{intercept}} \tag{4}$$

where $L_T$ is the transfer length.

When studying TLM structures with different dimensions or contact technologies, effective contact resistivity ($\rho_{c\text{-eff}}$) is an important figure of merit of the specific contact resistance in $\Omega{\cdot}\text{cm}^2$. Considering that $L \geq 1.5L_T$ for all our CuO TLM samples, $\rho_{c\text{-eff}}$ can be obtained by [19]

$$\rho_{c\text{-eff}} = R_{\text{sh}} \times L_T^2 = R_c A_{\text{eff}} = R_c W L_T \tag{5}$$

where the effective contact area ($A_{\text{eff}}$) is defined as $W \cdot L_T$. Reciprocally, $L_T$, indicating the average length along the electrode width used for the current transfer between CuO and Au, stresses the opposite influences of $\rho_{c\text{-eff}}$ and $R_{\text{sh}}$ [19]

$$L_T = \sqrt{\frac{\rho_{c\text{-eff}}}{R_{\text{sh}}}}. \tag{6}$$

### A. TLM Structures With Lower $R_{sh}$ Measured in $N_2$

CuO/Au TLM structures with a thick CuO of 830 nm were fabricated and characterized in $N_2$ flow with different contact geometries and CuO widths of Structures A–D. The measurements repeated on the three exact same Structures A and B of the layout exhibited close results. Taking Structure A as an example, typical current–voltage ($I$–$V$) curves of each pair of adjacent strips are given in Fig. 4(a). Linear fittings gave coefficients of determination ($r^2$) $> 0.9999$ for all the measured $I$–$V$ curves. For all the measurements in this work, similar $I$–$V$ curves were measured, passing linearly by the origin as expected for an ohmic contact and extremely low leakage currents. The corresponding total resistances were extracted at each applied bias by three-point derivatives. The values keep almost identical in the range of applied biases from $-1$ to 1 V and thus are arbitrarily presented at $-0.5$ V in what follows. The $R_T$–$d$ curves of Structures A and B with different strip widths of 25 and 50 $\mu$m are shown in Fig. 4(b). In addition to the contact geometry, Structures B–D with different CuO widths of 1000, 500, and 200 $\mu$m are further investigated in Fig. 4(c). $r^2$ on the linear regressions of results in Fig. 4(b) and (c) is over 0.99. From these very good linear fittings on the $R_T$–$d$ curves, the key parameters of CuO/Au TLM structures are extracted and listed in Table I according to (2)–(5).

TABLE I
EXTRACTED PARAMETERS OF STRUCTURES A–D MEASURED IN $N_2$ FLOW DIRECTLY AFTER FABRICATION

| Structure (Strip width, CuO Width) | A (25, 1000 um) | B (50, 1000 um) | C (50, 500 um) | D (50, 200 um) |
|---|---|---|---|---|
| $R_{sh}$ ($\Omega{\cdot}\text{sq}^{-1}$) | $1.20\times10^7$ | $1.29\times10^7$ | $1.9\times10^7$ | $1.94\times10^7$ |
| $R_c{\cdot}W$ ($\Omega{\cdot}$cm) | 2582.8 | 2659.9 | 3265.5 | 3190.5 |
| $L_T$ ($\mu$m) | 2.16 | 2.06 | 1.72 | 1.64 |
| $\rho_{c\text{-eff}}$ ($\Omega{\cdot}\text{cm}^2$) | 0.56 | 0.55 | 0.56 | 0.52 |

With regard to Structures A and B, $R_{\text{sh}}$ of CuO is $\sim 1.2 \times 10^7$ $\Omega{\cdot}\text{sq}^{-1}$, while the width normalized contact resistance ($R_c \cdot W$) between CuO and Au for both structures is about $\sim$2.6 k$\Omega{\cdot}$cm. $R_c \cdot W$ is relatively low compared to the total resistance of CuO, which confirms a good ohmic contact between CuO and Au, consistent with the linear $I$–$V$ curves. Considering different strip widths of 25 and 50 $\mu$m for Structures A and B, $L_T$ keeps almost the same to be $\sim$2.1 $\mu$m, which is much shorter than the strip width. These relatively wide electrodes have no influence on $R_c \cdot W$, so $R_c \cdot W$ is determined by the effective contact area instead of the physical contact size.

The hole mobility ($\mu$) of CuO can be estimated by: $\mu = 1/(pqR_{\text{sh}}t)$, where $p$, $q$, and $t$ are the hole concentration, electron charge, and CuO thickness, respectively. Considering a hole concentration of $\sim 3.92 \times 10^{14}$ $\text{cm}^{-3}$ obtained from the Hall measurement [6], $\mu$ in Structures A and B is calculated to be $\sim$15 $\text{cm}^2{\cdot}\text{V}^{-1}{\cdot}\text{s}^{-1}$, which is lower than a value of 34.2 $\text{cm}^2{\cdot}\text{V}^{-1}{\cdot}\text{s}^{-1}$ observed in the bulk CuO thin film [6]. Compared to the bare CuO thin film, the additional fabrication processes can affect the mobility of CuO. Here, lithography and Au deposition could lead to photoresist contamination and Au diffusion into CuO as two main sources of the mobility difference. Organic photoresist can indeed affect the CuO surface and introduce more defects in CuO during dc sputtering [20], [21]. According to the band alignment, a strong hole accumulation caused by Au diffusion can appear at the CuO/Au interface, resulting in an increase of the hole concentration in CuO [22]. The hole mobility would thus degrade at a higher hole concentration as established in [6]. Such external Au diffusion can easily cause a long-term degradation of semiconductor devices [23].

Comparing Structures C and D with Structure B, a slightly increased $R_{\text{sh}}$ of $\sim 1.9 \times 10^7$ $\Omega{\cdot}\text{sq}^{-1}$ and an increased $R_c \cdot W$ of $\sim$3.2 k$\Omega{\cdot}$cm are obtained, which again proves the repeatability and reliability of the measurements. Although processed simultaneously, these structures were measured several hours later than Structure B. In this duration, the sample was placed in a chamber with $N_2$ flow. However, the environmental influences could not be eliminated since the samples were not fully isolated from the environment during transportation to and in the chamber. Therefore, such phenomenon might indicate a slight alteration of the CuO thin film when exposed to air. Such an alteration is small and would not affect the conclusions

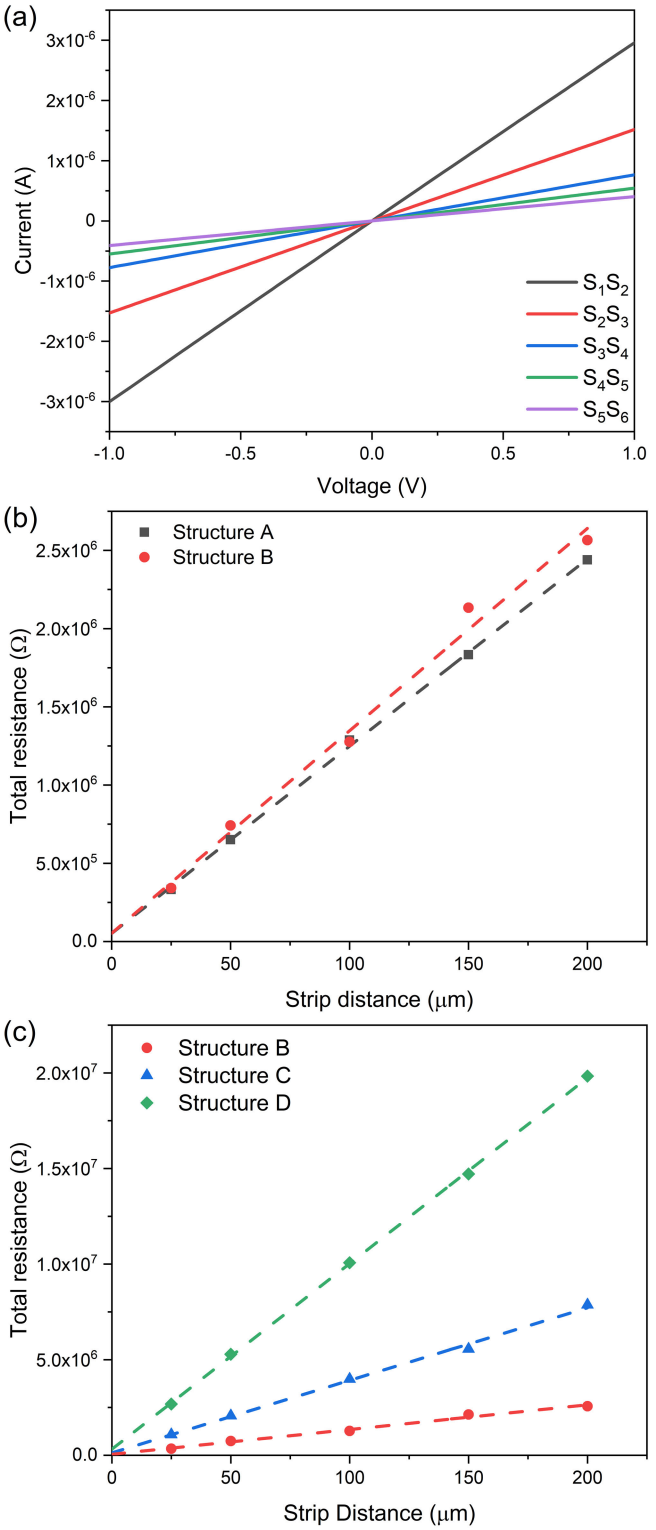


Fig. 4. (a) *I–V* curves for each pair of adjacent strips in Structure A. Total resistance versus strip distance of low-$R_{sh}$ CuO/Au TLM structures measured in $N_2$ (b) with different strip widths and (c) with different CuO widths.

of the measurement. Decreasing $W$ from 1000 to 200 $\mu$m, $R_c$ increases from 26 599 to 159 526 Ω due to the decreased contact size, which is consistent with (5). $L_T$ decreases from 2.06 to 1.72 and 1.64 $\mu$m with the decrease of $W$, mainly due to an increased $R_{sh}$. In addition, with the decrease of $W$, stronger fringing electrical fields around the edges of the diffused layer would affect the accuracy of the TLM and cause the decrease of $L_T$ [24]. To eliminate the influence from the contact size and have a standard quantity for comparison, similar $\rho_{c\text{-eff}}$ around 0.55 Ω·cm$^2$ is calculated for all structures by (5).

TABLE II
EXTRACTED PARAMETERS OF STRUCTURES A′ AND B′ MEASURED IN VACUUM

| Structure (Strip Width) | A' (25um) | B' (50um) |
|---|---|---|
| $R_{sh}$ (Ω·sq$^{-1}$) | 6.9×10$^7$ | 7.15×10$^7$ |
| $R_c$·$W$ (Ω·cm) | 1963.4 | 1756 |
| $L_T$ (μm) | 0.28 | 0.25 |
| $\rho_{c\text{-}eff}$ (Ω·cm$^2$) | 0.054 | 0.045 |

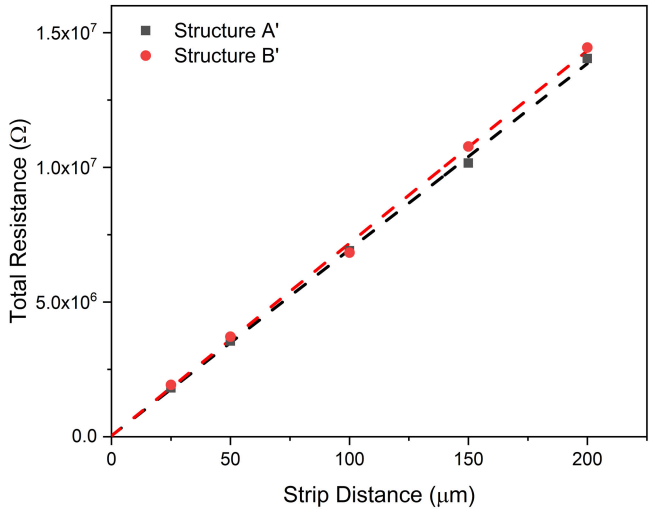


Fig. 5. Total resistance versus strip distance of higher $R_{sh}$ CuO/Au TLM structures with different strip widths measured in vacuum.

## B. TLM Structures With Higher $R_{sh}$ Measured in Vacuum

To figure out whether the degradation over time is influenced by a process intrinsic to CuO or by measurement conditions, other TLM structures (Structures A′ and B′ with the same dimensions as Structures A and B) have been fabricated and characterized in vacuum immediately after deposition. After a sputtering of 5 h, a CuO thickness of 750 nm was obtained, which is thinner than the previously sputtered CuO of 830 nm due to the consumption of Cu target and the decrease of discharge voltage. Given the repeatable and reliable measurements in $N_2$, the measurements in vacuum were conducted only once to minimize any possible aging and to control every time point precisely. Following *I–V* measurements in vacuum and extractions of corresponding resistance values, the $R_T$–$d$ curves of Structures A′ and B′ are shown in Fig. 5 and fitted by linear regressions with $r^2$ over 0.99. According to (2)–(5), the key parameters obtained by linear fittings of $R_T$–$d$ curves are given in Table II.

In vacuum, Structures A′ and B′ show a higher $R_{sh}$ of ~7 × 10$^7$ Ω·sq$^{-1}$ compared to Structures A and B due to a

TABLE III
EXTRACTED PARAMETERS OF STRUCTURE B′ MEASURED OVER 3-H AGING IN VACUUM AT ROOM TEMPERATURE

| Measurement time | 0 hour | 1 hour | 2 hours | 3 hours |
|---|---|---|---|---|
| $R_{sh}$ (Ω·sq$^{-1}$) | 7.15×10$^7$ | 7.68×10$^7$ | 9.6×10$^7$ | 1.09×10$^8$ |
| $R_c$·$W$ (Ω·cm) | 1756 | 29577.8 | 51221.5 | 61495.6 |
| $L_T$ (μm) | 0.25 | 3.85 | 5.34 | 5.64 |
| $\rho_{c\text{-}eff}$ (Ω·cm$^2$) | 0.045 | 11.38 | 27.37 | 34.67 |

different and thinner CuO film and to a potential degradation in air during a pumping of 2 h to achieve the target vacuum level. The $R_c \cdot W$ for Structures A′ and B′ is ∼1.8 kΩ·cm, which is lower compared to Structures A and B. As a result of an increase in $R_{sh}$ and a decrease in $L_T$ from ∼2.1 to ∼0.25 $\mu$m, $\rho_{c\text{-eff}}$ decreases from ∼0.55 to ∼0.05 Ω·cm$^2$, in coincidence with (5). At higher $R_{sh}$ and lower $\rho_{c\text{-eff}}$, the current quickly flows into the contact at the edge of the contact available for conduction [25]. In contrast, the current path is expanded at high $\rho_{c\text{-eff}}$, requiring a larger contact area for conduction. Similar $L_T$ in Structures A′ and B′ again proves that the wide electrodes have no influence on $R_c \cdot W$. These results again confirm the potential to obtain an initially very low contact resistivity between CuO and Au, no matter in $N_2$ flow or vacuum, but dependent on the sheet resistance. However, Structure B′ measured several minutes after Structure A′ already shows a slight increase of $R_{sh}$ and a further reduction of $L_T$ and $\rho_{c\text{-eff}}$ (Table II) similar to the results obtained in $N_2$ flow (Table I).

### C. Aging in Vacuum With Time and Temperature

The degradation of thin semiconductor layers is often influenced by environmental impacts, including temperature, moisture, and other mechanical, physical, or chemical influence from the fabrication and measurement environments. Among various elements, temperature is particularly important since most degradation mechanisms are thermally activated. The temperature variations in the device can be caused by the external heating or the self-heating.

1) Fig. 6 displays the $R_T$–$d$ curves of Structure B′ while maintained in vacuum at room temperature under dark to avoid other environmental influences and fitted by linear regressions with $r^2$ over 0.99 again. The first measurement noted "0 h" was taken after 2 h of pumping, and subsequent measurements were taken every hour thereafter. By linear fitting, the key parameters of Structure B′ measured in 3 h are extracted from $R_T$–$d$ curves in Table III by (2)–(5). The resistance between $S_1$ and $S_2$ increases from 1.92 × 10$^6$ to 3.82 × 10$^6$ Ω after 3 h in vacuum. $R_{sh}$ of CuO increases from 7.1 × 10$^7$ to 1.1 × 10$^8$ Ω·sq$^{-1}$ after 3 h in vacuum, while $\rho_{c\text{-eff}}$ of CuO/Au contact strongly degrades from 0.045 to 34.67 Ω·cm$^2$.

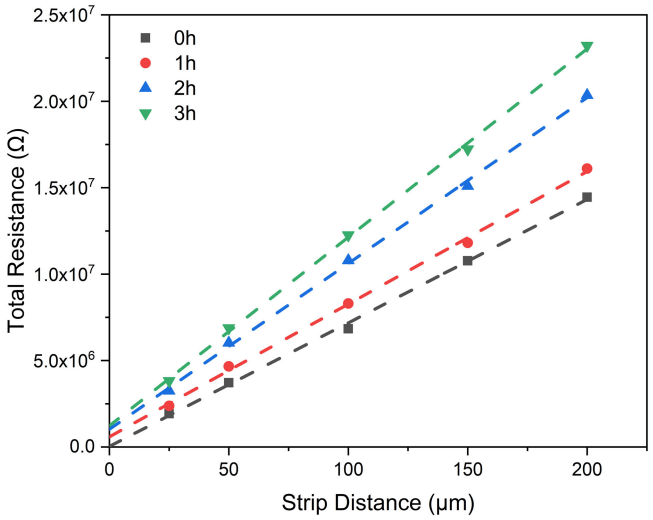


Fig. 6. Total resistance versus strip distance of Structure B′ measured over 3-h aging in vacuum at room temperature.

2) In order to further investigate the degradation of CuO TLM structures, Structure B′ was submitted to a high temperature of 100 °C in vacuum. Such method called dry heating measurement accelerates the device aging in a relatively short time. After heating up from 25 °C to 100 °C and stabilizing the temperature in vacuum, the electrical characteristics between $S_1$ and $S_2$ were measured at 100 °C every 30 min again, and the resistance between $S_1$ and $S_2$ was obtained as a function of time in Fig. 7(a). After 5 h at 100 °C, the resistance measured at 100 °C increases gradually from 9.24 × 10$^5$ to 3.19 × 10$^6$ Ω, showing a significant accelerated degradation of the CuO TLM structure. Finally, in Fig. 7(b), Structure B′ was remeasured in $N_2$ at room temperature after all these aging experiments. $R_T$–$d$ results were fitted by linear regressions with $r^2$ over 0.99 and compared with the first measurements done in Fig. 5. Strong degradations of $R_{sh}$ from 7.15 × 10$^7$ to 1.6 × 10$^9$ Ω·sq$^{-1}$ and $\rho_{c\text{-eff}}$ from 0.045 to 2.56 Ω·cm$^2$ were observed.

## IV. DISCUSSION

In summary, the degradation of CuO/Au TLM structures over time was first observed in $N_2$ and further studied in vacuum. During the measurement in vacuum at room temperature, environmental impacts, such as temperature, moisture, air exposure, and other mechanical, physical, or chemical influences from the fabrication and measurement environments, could be ignored. Therefore, the degradation could only be originated from the sample itself or from the self-heating during the measurement. However, the Joule heating during the measurement was too small to cause any temperature increase. Therefore, the degradations of both $R_{sh}$ and $\rho_{c\text{-eff}}$ might be attributed to the increase of defect states in CuO. More bulk defects with the aging of CuO reduce the hole mobility and cause an increase of $R_{sh}$. Increased interfacial defects at the CuO/Au contact can induce a Fermi pinning effect, frequently seen at interfaces with oxides [21], resulting

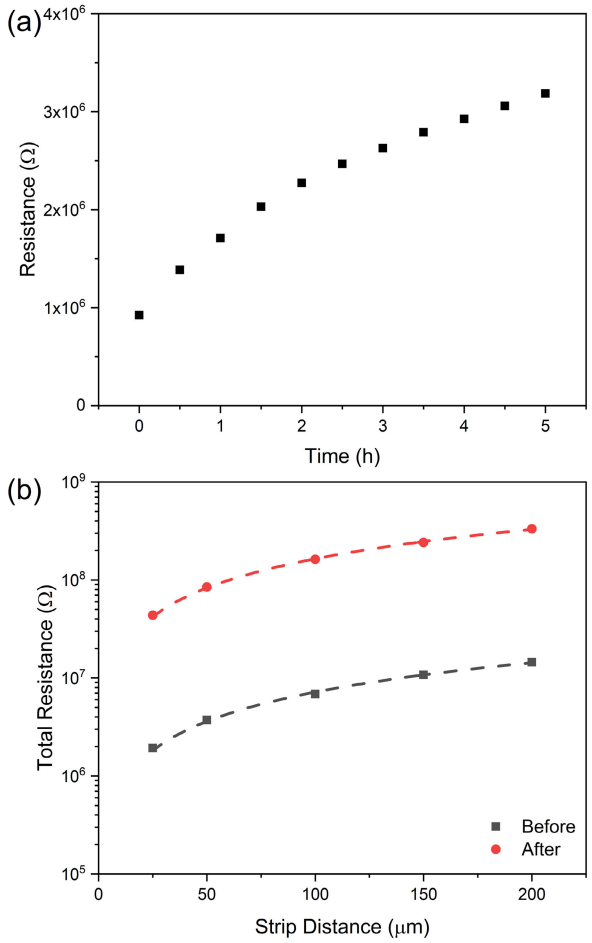


Fig. 7. (a) $S_1S_2$ resistance variation with time measured in vacuum at 100 °C in 5 h. (b) Total resistance versus strip distance of Structure B′ before and after all the measurements.

in an increased $\rho_{c\text{-eff}}$. The increase of bulk and interfacial defects could be attributed to the photoresist contamination, TLM structure, Au diffusion, or bias-stress and illumination during the measurement [26], [27]. Trapping and detrapping of charges in the defect states of CuO also result in a well-known long-term instability of CuO devices [27].

Next, as the temperature is increased, the total resistance typically decreases in the beginning of the aging measurement, showing a lower $S_1S_2$ resistance at 100 °C than that at 25 °C in Fig. 4. At high temperatures, more free carriers are indeed created after gaining enough thermal energy to overcome the bandgap [28]. This phenomenon contributes to the increase of carrier concentration in CuO and thus decreases the resistance. However, keeping the structure at 100 °C for a longer time, an additional degradation effect became dominant, demonstrating a significant increase of $S_1S_2$ resistance. At elevated temperatures, Na release from the SLG substrate and Na diffusivity from the SLG substrate into CuO would be greatly enhanced [29]. Na diffusion would create more bulk and interfacial defects like copper vacancies and oxygen vacancies at the grain boundaries of CuO [30]. As time passes at 100 °C, more defects in CuO could be created from Na diffusion, significantly accelerating the degradation process at high temperature.

TABLE IV
COMPARISON WITH LITERATURES

| Structure | $t_{CuO}$ (nm) | $R_{sh}$ (Ω·cm) | $\rho_{c\text{-}eff}$ (Ω·cm²) | $L_T$ (μm) |
|---|---|---|---|---|
| **CuO/Au [14]** | 470 | / | $1.05\times10^5$ | 87.7 |
| **CuO/Au [16]** | 175 | / | $2.1\times10^3$ | / |
| **Structure B' (Before)** | 750 | $7.15\times10^7$ | 0.045 | 0.25 |
| **Structure B' (After)** | 750 | $1.6\times10^9$ | 2.56 | 0.4 |

Finally, compared with top-contact CuO/Au TLM structures reported in literature (Table IV), a record low $\rho_{c\text{-eff}}$ of only 0.045 Ω·cm² is obtained in this work for bottom-contact CuO/Au TLM structures measured in vacuum just after fabrication (Structure B′ ), which is $2.3 \times 10^6$ and $4.7 \times 10^4$ times lower than [14] and [16]. Such a low $\rho_{c\text{-eff}}$ is also close to a standard value of less than 0.08 Ω·cm² for CIGS/$MoSe_2$ [31], [32] and much lower than other metal contacts with copper oxides like $Cu_2O$/Au and $Cu_2O$/Ni TLM structures with values over $10^3$ Ω·cm² in [12] and [16]. The improvements reported in this work might be attributed to two possible hypotheses.

1) The degradation of the CuO/Au interface and the growth of a thin oxidized film at the interface are more pronounced in top-contact TLM structures. Such an interfacial layer might be reduced in this work as we deposited CuO after Au patterning to avoid exposing the CuO/Au interface directly to the air, when CuO surface can absorb oxygen molecules, resulting in the formation of electron traps and a thin oxidized film, degrading the device performance [33].
2) A higher $R_{sh}$ and hence a lower doping level of a few $10^{14}$ $cm^{-3}$ in this work lead to a better ohmic contact between CuO with a workfunction ($\varphi$) estimation of 5.3 eV and Au ($\varphi$ = 5.47 eV). On the contrary, widely reported higher p-type doping levels, e.g., ~$5 \times 10^{17}$ $cm^{-3}$ ($\varphi$ = 5.49 eV) in [9] and $2.3 \times 10^{16}$ $cm^{-3}$ in [16], would lead to a CuO/Au contact featuring a barrier to hole conduction and hence much increased contact resistivity.

After initial measurements, Structure B′ experienced a long-time degradation process in vacuum, including 3 h of room-temperature (25 °C) aging, heating up from 25 °C to 100 °C, 5 h of high-temperature (100 °C) aging, and cooling down to 25 °C. Even after such a strong stress experiment, $\rho_{c\text{-eff}}$ of Structure B′ obtained in this work is still $4.1 \times 10^4$ and $8.2 \times 10^2$ times lower than [14] and [16].

## V. CONCLUSION

Due to a cleaner CuO/Au interface and a lower CuO doping level, CuO/Au TLM structures are optimized both in $N_2$ and vacuum by bottom-contact structures with Au evaporation prior to CuO sputtering. Considering different metal strip widths and CuO widths, our measurements consistently reveal an ohmic contact between CuO with Au. The initial effective contact resistivity ranges from a low value of ~0.55 Ω·cm² for the structures featuring a CuO thickness of 830 nm and

$R_{sh}$ of $\sim 1.2 \times 10^7$ $\Omega \cdot sq^{-1}$ measured in $N_2$ to a record low value of $\sim 0.05$ $\Omega \cdot cm^2$ for the structures featuring a CuO thickness of 750 nm and $R_{sh}$ of $\sim 7 \times 10^7$ $\Omega \cdot sq^{-1}$ measured in vacuum.

Furthermore, the degradations of bottom-contact CuO/Au TLM structures in vacuum are observed with time and discussed for the first time. An increase of the sheet resistance of CuO by a factor of 1.53 after 3 h in vacuum at room temperature indicates the degradation. This degradation in vacuum is significantly accelerated at 100 °C. With regard to the effective contact resistivity, a strong degradation was observed in vacuum at room temperature, finally reaching 2.56 $\Omega \cdot cm^2$ when remeasured in $N_2$ at room temperature after all the high-temperature aging experiments. Potential relations of our observations with different degradation mechanisms have been discussed. Therefore, it is important in future works to further study how to limit the environmental degradation of CuO structures, e.g., by introducing a top passivation layer.

## REFERENCES


[1] D. Liu, G. Yang, Y. Zhao, N. Lu, J. Wang, and L. Li, "Decoupling the roles of thermionic and field emissions in contact resistance of field effect transistors," *IEEE Electron Device Lett.*, vol. 43, no. 7, pp. 1065–1068, Jul. 2022, doi: 10.1109/LED.2022.3172569.

[2] Y. Du, H. Liu, Y. Deng, and P. D. Ye, "Device perspective for black phosphorus field-effect transistors: Contact resistance, ambipolar behavior, and scaling," *ACS Nano*, vol. 8, no. 10, pp. 10035–10042, Oct. 2014, doi: 10.1021/nn502553m.

[3] S. Knobelspies, A. Takabayashi, A. Daus, G. Cantarella, N. Münzenrieder, and G. Tröster, "Improvement of contact resistance in flexible a-IGZO thin-film transistors by $CF_4/O_2$ plasma treatment," *Solid-State Electron.*, vol. 150, pp. 23–27, Dec. 2018, doi: 10.1016/j.sse.2018.10.002.

[4] S. H. Rha et al., "Performance variation according to device structure and the source/drain metal electrode of a-IGZO TFTs," *IEEE Trans. Electron Devices*, vol. 59, no. 12, pp. 3357–3363, Dec. 2012, doi: 10.1109/TED.2012.2220367.

[5] H. Mir, V. Arya, H. Höffler, and A. Brand, "A novel TLM analysis for solar cells," *IEEE J. Photovolt.*, vol. 9, no. 5, pp. 1336–1342, Sep. 2019, doi: 10.1109/JPHOTOV.2019.2923337.

[6] X. Zeng, M. Zhukova, S. Faniel, J. Proost, and D. Flandre, "Structural and opto-electronic characterization of CuO thin films prepared by DC reactive magnetron sputtering," *J. Mater. Sci., Mater. Electron.*, vol. 31, no. 6, pp. 4563–4573, Mar. 2020, doi: 10.1007/s10854-020-03007-4.

[7] W. Zheng, Y. Chen, X. Peng, K. Zhong, Y. Lin, and Z. Huang, "The phase evolution and physical properties of binary copper oxide thin films prepared by reactive magnetron sputtering," *Materials*, vol. 11, no. 7, p. 1253, Jul. 2018, doi: 10.3390/ma11071253.

[8] H. L. Skriver and N. M. Rosengaard, "Surface energy and work function of elemental metals," *Phys. Rev. B, Condens. Matter*, vol. 46, no. 11, pp. 7157–7168, Sep. 1992, doi: 10.1103/physrevb.46.7157.

[9] X. Zeng, M. Zhukova, S. Faniel, G. Li, and D. Flandre, "Room-temperature DC-sputtered p-type CuO accumulation-mode thin-film transistors gated by $HfO_2$," *Appl. Phys. Lett.*, vol. 121, no. 13, Sep. 2022, Art. no. 133503, doi: 10.1063/5.0098757.

[10] M. Napari et al., "Role of ALD $Al_2O_3$ surface passivation on the performance of p-type $Cu_2O$ thin film transistors," *ACS Appl. Mater. Interfaces*, vol. 13, no. 3, pp. 4156–4164, Jan. 2021, doi: 10.1021/acsami.0c18915.

[11] S. Lee et al., "Sol-gel processed p-type CuO phototransistor for a near-infrared sensor," *IEEE Electron Device Lett.*, vol. 39, no. 1, pp. 47–50, Jan. 2018, doi: 10.1109/LED.2017.2779816.

[12] J. Jo, J. D. Lenef, K. Mashooq, O. Trejo, N. P. Dasgupta, and R. L. Peterson, "Causes of the difference between Hall mobility and field-effect mobility for p-type RF sputtered $Cu_2O$ thin-film transistors," *IEEE Trans. Electron Devices*, vol. 67, no. 12, pp. 5557–5563, Dec. 2020, doi: 10.1109/TED.2020.3033832.

[13] D. K. Schroder, *Semiconductor Material and Device Characterization*, 3rd ed., Hoboken, NJ, USA: Wiley, 2006, doi: 10.1002/0471749095.

[14] A. Akkaya, O. Kahveci, R. Aydın, and B. Şahin, "Amplifying main physical characteristics of CuO films using ascorbic acid as the reducer and stabilizer agent," *Appl. Phys. A, Mater. Sci. Process.*, vol. 127, no. 12, p. 911, Dec. 2021, doi: 10.1007/s00339-021-05078-4.

[15] A. Mudhaffar, B. Sultan, E. Shalaan, and H. Al-Jawhari, "Switching enhancement in copper oxide thin-film transistors via molybdenum trioxide buffering and nitrogen doping," *J. Electron. Mater.*, vol. 52, no. 5, pp. 3446–3454, May 2023, doi: 10.1007/s11664-023-10334-9.

[16] V. Singh, J. Sinha, and S. Avasthi, "Two-step process using MOCVD and thermal oxidation to obtain pure-phase $Cu_2O$ thin films transistors," *ACS Appl. Electron. Mater.*, vol. 4, no. 1, pp. 367–374, Jan. 2022, doi: 10.1021/acsaelm.1c01050.

[17] A. Kumar, H. Singh, S. Sahay, and K. B. Balasubramanian, "Charge injection into electrodeposited $Cu_2O$ from metallic stacks and graphene," *IEEE Trans. Electron Devices*, vol. 69, no. 10, pp. 5755–5759, Oct. 2022, doi: 10.1109/TED.2022.3197380.

[18] J. Cha, J. Son, and J. Hong, "A bottom-electrode contact: The most suitable structure for graphene electronics," *Adv. Mater. Interfaces*, vol. 9, no. 6, Jan. 2022, Art. no. 2102207, doi: 10.1002/admi.202102207.

[19] S. Guo, G. Gregory, A. M. Gabor, W. V. Schoenfeld, and K. O. Davis, "Detailed investigation of TLM contact resistance measurements on crystalline silicon solar cells," *Sol. Energy*, vol. 151, pp. 163–172, Jul. 2017, doi: 10.1016/j.solener.2017.05.015.

[20] M. Mashock, K. Yu, S. Cui, S. Mao, G. Lu, and J. Chen, "Modulating gas sensing properties of CuO nanowires through creation of discrete nanosized p–n junctions on their surfaces," *ACS Appl. Mater. Interfaces*, vol. 4, no. 8, pp. 4192–4199, Aug. 2012, doi: 10.1021/am300911z.

[21] S. Liu et al., "Nanopatterning technologies of 2D materials for integrated electronic and optoelectronic devices," *Adv. Mater.*, vol. 34, no. 52, Dec. 2022, Art. no. 2200734, doi: 10.1002/adma.202200734.

[22] J. Morasch, H. F. Wardenga, W. Jaegermann, and A. Klein, "Influence of grain boundaries and interfaces on the electronic structure of polycrystalline CuO thin films," *Phys. Status Solidi Appl. Mater. Sci.*, vol. 213, no. 6, pp. 1615–1624, Jun. 2016, doi: 10.1002/pssa.201533018.

[23] K. Domanski et al., "Not all that glitters is gold: Metal-migration-induced degradation in perovskite solar cells," *ACS Nano*, vol. 10, no. 6, pp. 6306–6314, Jun. 2016, doi: 10.1021/acsnano.6b02613.

[24] S. Grover, S. Sahu, P. Zhang, K. O. Davis, and S. K. Kurinec, "Standardization of specific contact resistivity measurements using transmission line model (TLM)," in *Proc. IEEE 33rd Int. Conf. Microelectron. Test Struct. (ICMTS)*, May 2020, pp. 1–6, doi: 10.1109/ICMTS48187.2020.9107911.

[25] P. Zhang, Y. Y. Lau, and R. M. Gilgenbach, "Analysis of current crowding in thin film contacts from exact field solution," *J. Phys. D, Appl. Phys.*, vol. 48, no. 47, Dec. 2015, Art. no. 475501, doi: 10.1088/0022-3727/48/47/475501.

[26] J.-H. Lee, Y.-J. Choi, C.-Y. Jeong, D.-K. Jung, S. Ham, and H.-I. Kwon, "Electrical instability of p-channel SnO thin-film transistors under light illumination," *IEEE Electron Device Lett.*, vol. 37, no. 3, pp. 295–298, Mar. 2016, doi: 10.1109/LED.2016.2516578.

[27] I.-C. Chiu and I.-C. Cheng, "Gate-bias stress stability of p-type SnO thin-film transistors fabricated by RF-sputtering," *IEEE Electron Device Lett.*, vol. 35, no. 1, pp. 90–92, Jan. 2014, doi: 10.1109/LED.2013.2291896.

[28] A. D. Faisal and W. K. Khalef, "Morphology and structure of CuO nanostructures grown via thermal oxidation on glass, silicon, and quartz at different oxidation temperatures," *J. Mater. Sci., Mater. Electron.*, vol. 28, no. 24, pp. 18903–18912, Dec. 2017, doi: 10.1007/s10854-017-7844-z.

[29] P. Salomé, V. Fjällström, A. Hultqvist, and M. Edoff, "Na doping of CIGS solar cells using low sodium-doped mo layer," *IEEE J. Photovolt.*, vol. 3, no. 1, pp. 509–513, Jan. 2013, doi: 10.1109/JPHOTOV.2012.2226144.

[30] H. Siddiqui, M. R. Parra, M. S. Qureshi, M. M. Malik, and F. Z. Haque, "Studies of structural, optical, and electrical properties associated with defects in sodium-doped copper oxide (CuO/Na) nanostructures," *J. Mater. Sci.*, vol. 53, no. 12, pp. 8826–8843, Jun. 2018, doi: 10.1007/s10853-018-2179-6.

[31] L. Assmann, J. C. Bernède, A. Drici, C. Amory, E. Halgand, and M. Morsli, "Study of the mo thin films and Mo/CIGS interface properties," *Appl. Surf. Sci.*, vol. 246, nos. 1–3, pp. 159–166, Jun. 2005, doi: 10.1016/j.apsusc.2004.11.020.

[32] J. Yoon et al., "Electrical properties of CIGS/Mo junctions as a function of $MoSe_2$ orientation and Na doping," *Prog. Photovolt., Res. Appl.*, vol. 22, no. 1, pp. 90–96, Jan. 2014, doi: 10.1002/pip.2377.

[33] W. Yin et al., "High responsivity and external quantum efficiency photodetectors based on solution-processed Ni-doped CuO films," *ACS Appl. Mater. Interfaces*, vol. 12, no. 10, pp. 11797–11805, Mar. 2020, doi: 10.1021/acsami.9b18663.